ChemComm

COMMUNICATION

View Article Online
View Journal | View Issue

Cite this: *Chem. Commun.*, 2016, 52, 2165

Received 10th December 2015,
Accepted 16th December 2015

DOI: 10.1039/c5cc10145j

www.rsc.org/chemcomm

Hierarchical mesoporous silica nanoparticles as superb light scattering materials†

Jaehoon Ryu, Juyoung Yun, Jungsup Lee, Kisu Lee and Jyongsik Jang*

A novel approach to enhance the light scattering effect was explored by applying hierarchical silica nanoparticles in DSSCs as scattering layers. The WSN-incorporated cells showed a PCE value of 9.53% and a PCE enhancement of 30.19% compared with those of the reference cells.

Hierarchical nanomaterials have recently attracted a great deal of interest in terms of overcoming the disadvantages associated with conventional methods that use large particles for light scattering in dye-sensitized solar cells (DSSCs).[1–8] The porous nature of hierarchical nanomaterials provides a large surface area in spite of the large diameter, which enhances the light scattering and dye-loading capabilities of the materials. Moreover, hierarchical nanomaterials effectively reduce the required working electrode thickness, consequently, leading to suppressed charge recombination.[9] For these reasons, many studies have focused on the formation of a mesoporous semiconducting layer consisting of hierarchically-structured TiO_2 (or ZnO) without separation of a nanocrystalline layer and a light scattering layer, leading to considerable enhancement of cell performances.[10–13] However, most of the approaches for manufacturing hierarchical nanomaterials based on TiO_2 (or ZnO) involve solvothermal (or hydrothermal) processes, which limits large-scale production and still has difficulty in practical or industrial applications.

Comparable to TiO_2, various synthetic approaches for fabricating hierarchical SiO_2 nanoparticles have been recently developed (*e.g.*, biphase stratification and micro- or macro-emulsion template methods based on sol–gel chemistry).[14–19] These methods allow not only mass production, but also practical or industrial applications. Furthermore, the approaches could regulate particle and pore size, leading to a fairly large surface area (>500 m^2 g^{-1}).[20] These values presented are much larger than those of most hierarchical nanomaterials based on TiO_2 (or ZnO) (<200 m^2 g^{-1}). It indicates that the highly porous materials with large size could have potential for effective light scattering materials. However, despite its outstanding features, application of SiO_2 to DSSCs has been limited by the high conduction band energy of SiO_2 and thus, is yet to be reported. Hence, the use of hierarchical SiO_2 nanoparticles in DSSCs is challenging; however, if successful, a significant enhancement in DSSC performance is expected.

Herein, we fabricated hierarchical mesoporous silica nanoparticles with a radial wrinkle structure (WSNs) by micro-emulsion techniques for DSSCs as scattering layers. SiO_2 nanoparticles were coated with a thin layer of TiO_2 *via* $TiCl_4$ post-treatment to make the most of the dye usable, which is adsorbed onto the surface of WSNs coated with a thin layer of TiO_2. To the best of our knowledge, this is the first attempt to apply hierarchical silica nanoparticles in DSSC devices. Furthermore, the effect of the surface morphology of spherical particles on light scattering was investigated by comparing the light scattering capabilities of the WSNs with sphere-shaped SiO_2 nanoparticles of the same size. Importantly, our results demonstrated that WSNs stand out as outstanding light scattering materials, providing large surface area as well as multiple scattering by the hierarchical structure.

Fig. 1a shows a schematic illustration of the assembled DSSCs with a WSN scattering layer on the TiO_2 nanoparticle

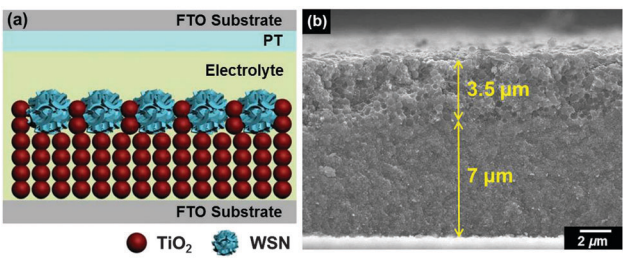

Fig. 1 (a) Schematic illustration and (b) cross-section SEM image of the device structure of DSSCs containing TiO_2 NP under-layers and WSN over-layers as scattering layers.

School of Chemical and Biological Engineering, College of Engineering, Seoul National University (SNU), Seoul, Korea. E-mail: jsjang@plaza.snu.ac.kr; Fax: +82 2 888 1604; Tel: +82 2 880 7069

† Electronic supplementary information (ESI) available: Detailed experimental procedures and supporting figures. See DOI: 10.1039/c5cc10145j

(NP) film of a working electrode. Additionally, pristine TiO_2 NPs and sphere-shaped SiO_2 NPs were also applied to the mesoporous film of a working electrode to investigate the effect of light scattering capabilities of the WSNs on the performance of DSSCs. The overall thickness of the mesoporous film was controlled to ~10–11 μm. A cross-sectional scanning electron microscopy (SEM) image of the device structure is shown in Fig. 1b; the thicknesses of the TiO_2 NP underlayer and overlayer (as scattering layers) were ~7 μm and ~3.5 μm, respectively. In the mixed structure consisting of WSNs and TiO_2 as scattering layers, the WSNs were dispersed uniformly without any brokenness (Fig. S1, ESI†).

WSNs were fabricated using the bicontinuous microemulsion phase of the Winsor III system.[18] The Winsor III system could be formed by selection of a specific mixture ratio of cyclohexane and an aqueous solution containing urea, CPB, and alcohol. Fig. 2 shows transmission electron microscopy (TEM) and SEM images of *ca.* 220, 320, and 430 nm-diameter WSNs (hereafter referred to as 220 WSNs, 320 WSNs, and 430 WSNs, respectively). The size of the WSNs can be controlled by the reaction heating time; specifically, 220, 320, and 430 WSNs were fabricated using reaction heating times of 8, 10, and 16 h, respectively. Thus, the size of the WSNs increased with the heating time. However, after 20 h of heating, the size of the WSNs was *ca.* 430 nm, similar to the size after 16 h of heating (Fig. S2, ESI†). The reduction in the growth rate

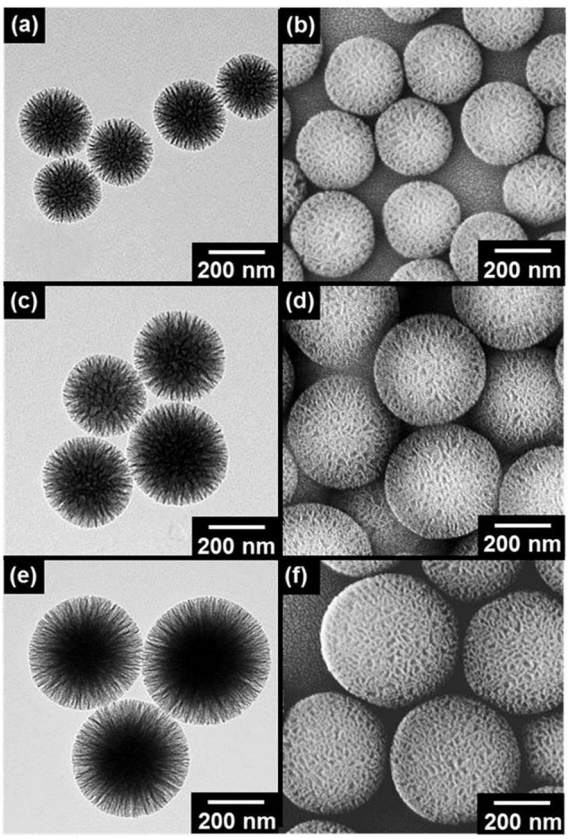

Fig. 2 TEM and SEM images of WSNs with diameters of *ca.* (a and b) 220 nm, (c and d) 320 nm, and (e and f) 430 nm.

Table 1 Summary of BET analysis of the silica spheres and WSNs with various sizes

Sample	BET area [m^2 g^{-1}]	Inter-wrinkle distance[a] [nm]
220 spheres	17.26	—
220 WSNs	572.09	10–20
320 WSNs	585.25	10–20
430 WSNs	592.85	10–20

[a] Corresponding to a wide peak in BJH pore distribution plots; there are two peaks in the BJH plot, consisting of a sharp peak (2 nm) and a wide band (*ca.* 15 nm)

with continued reaction heating was attributed to the change in pH of the reaction mixture;[18,19] the change in pH limited the size of the spherical particles. In this process, the pH of the mixture varied from 7 at the beginning of the reaction to 10 after 16 h of reaction time, with urea as the base catalyst. The Brunauer–Emmett–Teller (BET) surface areas of the WSNs were measured by N_2 adsorption–desorption isotherms; the surface area values are summarized in Table 1. The 220 WSNs exhibited a significantly enhanced specific surface area (572.09 m^2 g^{-1}) compared with that of SiO_2 spheres of the same size (17.26 m^2 g^{-1}). The surface area of the WSNs tended to increase with increasing particle size; however, only a slight difference was observed. The isotherms of the WSNs exhibited an H3-type hysteresis loop. Inter-wrinkle distances corresponding to the pore size of WSNs were confirmed to be ~15 nm by Barrett–Joyner–Halenda (BJH) adsorption pore distribution plots (Fig. S3, ESI†). These results can be explained by the slip shapes of the WSNs, as well as their mesoporous features.[21,22] Thus, these hierarchically structured materials were expected to not only increase dye loading *via* their extraordinary surface area but also provide superb light scattering capability.

Fig. 3a shows the diffuse reflectance spectra (DRS) of the prepared 220, 320, and 430 WSNs, and 220 nm SiO_2 spheres (hereafter referred to as 220 spheres, Fig. S4, ESI†). The 220 WSNs exhibited high reflectance over the range of 400–900 nm compared with sphere-shaped SiO_2 nanoparticles of the same size; light scattering was significantly enhanced by the hierarchical structure, as expected. Fig. 3b shows a comparison of the light scattering path in a SiO_2 sphere and a WSN. Multiple scattering events occurred at the numerous particle/air (electrolyte) interfaces of the WSNs *via* the hierarchical structure, leading to an increase in the light path length between neighboring particles.[23] Moreover, the reflectance in the visible-light regime increased with the size of the nanoparticles; this tendency was attributed to the size dependency of the light scattering effect.[24,25] Interestingly, the 220 nm-diameter nanoparticles (both the 220 spheres and 220 WSNs), 320 WSNs, and 430 WSNs showed characteristic reflectance peaks near 450 nm, 700 nm, and 850 nm, respectively.[26] These peaks were close to those predicted by Mie scattering theory, which states that the size of the spherical scatterer for effective light scattering is approximately half the wavelength of the incident light.[27]

Fig. 4 shows the photovoltaic performance of the assembled DSSCs with an anode film that incorporated 220 spheres,

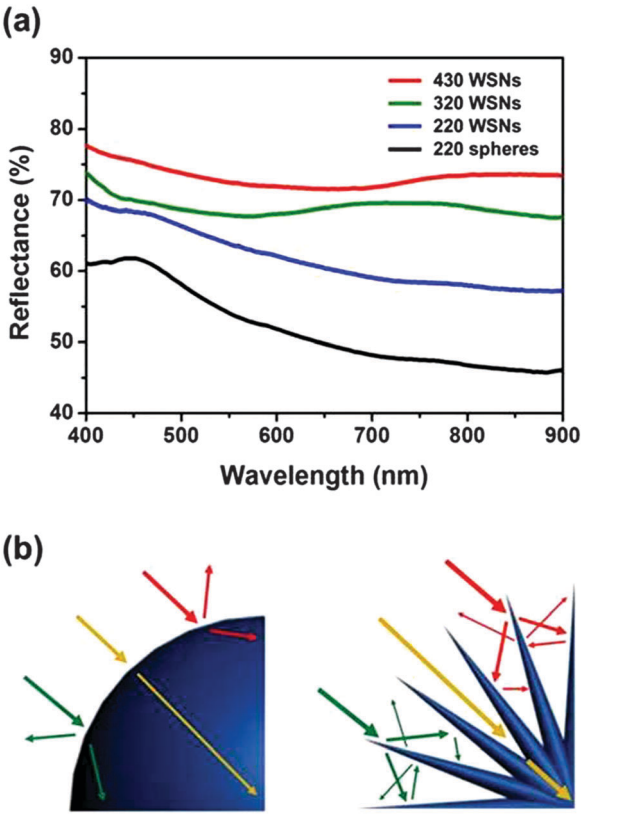

Fig. 3 (a) Diffused reflectance spectra of 220 nm silica spheres and WSNs with various sizes (220, 320, 430 nm). (b) Schematic illustration of the light scattering effect within spheres and WSNs.

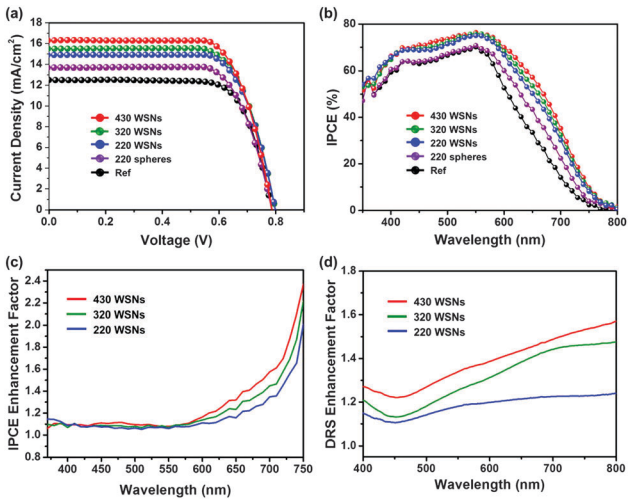

Fig. 4 (a) Current density–voltage (*J*–*V*) characteristics and (b) incident photon-to-current efficiency (IPCE) spectra of DSSCs based on WSNs with various sizes and 220 nm silica spheres; (c) IPCE enhancement factor (=$IPCE_{sample}/IPCE_{220spheres}$) and (d) DRS enhancement factor (=$DRS_{sample}/DRS_{220spheres}$) based on the 220 spheres.

220 WSNs, 320 WSNs, and 430 WSNs; the photovoltaic properties are summarized in Table 2. A remarkable difference in the short-circuit current (J_{sc}) was observed; however, the open-circuit voltage (V_{oc}) and fill factor (FF) values of all samples were similar. Compared with the reference cells (12.51 mA cm^{-2}), the J_{sc} values for the 220 spheres (13.71 mA cm^{-2}) and 220 WSNs (14.89 mA cm^{-2}) showed an enhancement of 9.59% and 19.02%, respectively, due to the light scattering effect produced by incorporating large SiO_2 nanoparticles. The extent of J_{sc} improvement with the 220 WSNs was much higher than that with the 220 spheres, compared with the reference device. As discussed above in Fig. 3b, multiple light scattering by the hierarchical structure increased the light path length and induced optical confinement. In addition, the significant improvement in the J_{sc} value of WSNs compared with SiO_2 spheres also contributed to the enhanced dye adsorption *via* a larger surface area. The higher conduction band of SiO_2 could prevent electrons generated by oxidation of the dye from transferring to the working electrode. However, the WSNs were easily coated with a thin TiO_2 layer through $TiCl_4$ post-treatment,[28] a well-known method, leading to electron transfer from the dye adsorbed to the surface of the SiO_2 coated with the TiO_2 layer to nanocrystalline TiO_2 particles.[29] Remarkable differences of XRD spectra between WSNs before and after $TiCl_4$ treatment were not observed (Fig. S5, ESI†). However, the HR-TEM image of WSNs after $TiCl_4$ treatment represented 0.34 nm lattice spacing corresponding to the [101] plane of anatase TiO_2 (Fig. S6, ESI†).[30] It demonstrated that the thin TiO_2 layer was coated onto the surface of WSNs. This can also be confirmed through BET analysis and DRS spectra of $TiCl_4$ treated-WSNs. The BET areas of WSNs after $TiCl_4$ treatment, which are summarized in Table S1 (ESI†), appear to be slightly smaller than those of WSNs. However, inter-wrinkle distances of $TiCl_4$ treated-WSNs were confirmed to be similar to those of WSNs before $TiCl_4$ treatment (Fig. S7, ESI†). In addition, DRS of $TiCl_4$ treated-WSNs presented similar trends, but slightly enhanced reflectance in the overall range compared with WSNs before $TiCl_4$ treatment (Fig. S8, ESI†). These results of BET and DRS indicate that a thin TiO_2 layer was coated on the surface of SiO_2 materials through $TiCl_4$ treatment and the enhancement of DRS intensity was attributable to the presence of high refractive index TiO_2 (=2.49) on the surface of SiO_2 (=1.47).[25] The J_{sc} value for WSN-incorporated cells increased with the WSN size, thus leading to an enhancement in the power conversion efficiency (PCE). The 430 WSNs showed the best photovoltaic performance under our experimental conditions, specifically a PCE value of 9.53% and a PCE enhancement of 30.19% compared with that of the reference cells.

Table 2 Summary of photovoltaic properties of WSNs and silica sphere-based DSSCs

Sample[a]	J_{sc} [mA cm^{-2}]	V_{oc} [V]	FF	η^b [%]
Ref[c]	12.51	0.79	0.74	7.32
220 spheres	13.71	0.79	0.74	7.92
220 WSNs	14.89	0.80	0.75	9.01
320 WSNs	15.50	0.80	0.75	9.32
430 WSNs	16.31	0.79	0.74	9.53

[a] Active area of the assembled DSSC samples is 0.16 cm^2. [b] Power conversion efficiency. [c] DSSC sample assembled without the scattering layer.

This J_{sc} variation was also confirmed by the incident photon-to-current efficiency (IPCE) spectra (Fig. 4b). The 220 WSNs showed a higher QE over the entire wavelength range compared with that of 220 spheres of the same size. It is also confirmed through IPCE enhancement factors based on the 220 spheres (Fig. 4c). A sharp increase was noticeable in the long wavelength region (>550 nm).[31] It is a similar tendency to the DRS enhancement factor based on 220 spheres, which increased with increasing wavelength (Fig. 4d). The N719 dye showed low absorbance in the long wavelength region, indicating that the adsorption amount of the dye is not an important factor in this wavelength region.[29] Therefore, this could explain that the influence of light scattering on IPCE is dominant in the long wavelength region. Meanwhile, despite large differences in DRS enhancement factor values of various sized WSNs in the short wavelength region (<550 nm), IPCE enhancement factors of all samples were kept at *ca.* 1.1 in the short wavelength region. It indicates that the intensity of light scattering would not largely affect the IPCE in the short wavelength region. However, if light scattering occurs in the short wavelength region, no matter how strong the intensity is, N719 can easily absorb light, as the dye showed strong light absorbance in this wavelength region. Interestingly, the amount of the dye adsorbed on the 220 WSNs was about 1.09 times higher than that adsorbed on the 220 spheres (Table S2, ESI†), which coincides with the IPCE enhancement factor of WSNs (=*ca.* 1.1) in the short wavelength region. Hence, the adsorption amount of the dye could be a critical factor in the short wavelength region in the presence of a certain extent of light scattering effect. Thus, WSNs provide an exceptional light scattering ability as well as a large surface area, compared with 220 spheres. Moreover, the QE value in IPCE data tended to increase with the particle size, especially in the long wavelength region. Thus, light scattering depends on the size of the WSNs, given similar BET areas. On the other hand, even though the dye-loading amount of 220 spheres was lower than that of reference cells due to the lower surface area, 220 spheres showed a similar QE value to reference cells in the short wavelength region. This could be explained by the fact that the scattering effect, which was not observed in reference cells, could make up for the loss due to the lower surface area. Therefore, the light scattering effect can influence the IPCE value over the entire region, but dye adsorption is the critical factor in the short wavelength region regardless of the light scattering intensity when a certain extent of light scattering occurs.

In conclusion, a simple and reliable strategy to introduce WSNs in DSSCs as scattering layers has been reported. $TiCl_4$ post-treatment played a key role as a method in the application of SiO_2 materials to DSSCs. WSN-incorporated cells show a 30.19% greater photovoltaic performance compared with pristine cells. This novel approach, which incorporates WSNs in DSSCs for the first time, is expected to advance the application of hierarchical SiO_2 materials to photovoltaic devices for improved performance.

This work was supported by the Global Frontier R&D Program on Center for Multiscale Energy System funded by the National Research Foundation under the Ministry of Science, ICT & Future Planning, Korea (2011-0031573).

Notes and references

1 H. Han, P. Sudhagar, T. Song, Y. Jeon, I. Mora-Sero, F. Fabregat-Santiago, J. Bisquert, Y. S. Kang and U. Paik, *Chem. Commun.*, 2013, **49**, 2810–2812.
2 Y. Li, Z. Che, X. Sun, J. Dou and M. Wei, *Chem. Commun.*, 2014, **50**, 9769–9772.
3 H. Mirabolghasemi, N. Liu, K. Lee and P. Schmuki, *Chem. Commun.*, 2013, **49**, 2067–2069.
4 J. Yang, C. Bao, K. Zhu, T. Yu, F. Li, J. Liu, Z. Li and Z. Zou, *Chem. Commun.*, 2014, **50**, 4824–4826.
5 P. Zhu, M. V. Reddy, Y. Wu, S. Peng, S. Yang, A. S. Nair, K. P. Loh, B. V. R. Chowdari and S. Ramakrishna, *Chem. Commun.*, 2012, **48**, 10865–10867.
6 H.-Y. Chen, Y.-F. Xu, D.-B. Kuang and C.-Y. Su, *Energy Environ. Sci.*, 2014, **7**, 3887–3901.
7 H.-B. Kim, H. Kim, W. I. Lee and D.-J. Jang, *J. Mater. Chem. A*, 2015, **3**, 9714–9721.
8 W.-Q. Wu, Y.-F. Xu, H.-S. Rao, C.-Y. Su and D.-B. Kuang, *J. Am. Chem. Soc.*, 2014, **136**, 6437–6445.
9 M. Planells, L. Pelleja, J. N. Clifford, M. Pastore, F. De Angelis, N. Lopez, S. R. Marder and E. Palomares, *Energy Environ. Sci.*, 2011, **4**, 1820–1829.
10 J. Lin, A. Nattestad, H. Yu, Y. Bai, L. Wang, S. X. Dou and J. H. Kim, *J. Mater. Chem. A*, 2014, **2**, 8902–8909.
11 Z. Li, Y. Zhou, G. Xue, T. Yu, J. Liu and Z. Zou, *J. Mater. Chem.*, 2012, **22**, 14341–14345.
12 W. Yang, J. Li, Y. Wang, F. Zhu, W. Shi, F. Wan and D. Xu, *Chem. Commun.*, 2011, **47**, 1809–1811.
13 S. H. Ahn, D. J. Kim, W. S. Chi and J. H. Kim, *Adv. Funct. Mater.*, 2014, **24**, 5037–5044.
14 V. Polshettiwar, D. Cha, X. Zhang and J. M. Basset, *Angew. Chem., Int. Ed.*, 2010, **49**, 9652–9656.
15 Y. Choi, Y. S. Yun, H. Park, D. S. Park, D. Yun and J. Yi, *Chem. Commun.*, 2014, **50**, 7652–7655.
16 P.-J. Chen, S.-H. Hu, W.-T. Hung, S.-Y. Chen and D.-M. Liu, *J. Mater. Chem.*, 2012, **22**, 9568–9575.
17 K. Zhang, L.-L. Xu, J.-G. Jiang, N. Calin, K.-F. Lam, S.-J. Zhang, H.-H. Wu, G.-D. Wu, B. Albela, L. Bonneviot and P. Wu, *J. Am. Chem. Soc.*, 2013, **135**, 2427–2430.
18 D.-S. Moon and J.-K. Lee, *Langmuir*, 2012, **28**, 12341–12347.
19 D. Shen, J. Yang, X. Li, L. Zhou, R. Zhang, W. Li, L. Chen, R. Wang, F. Zhang and D. Zhao, *Nano Lett.*, 2014, **14**, 923–932.
20 X. Du and S. Z. Qiao, *Small*, 2015, **11**, 392–413.
21 T. Yang, R. Zhou, D.-W. Wang, S. P. Jiang, Y. Yamauchi, S. Z. Qiao, M. J. Monteiro and J. Liu, *Chem. Commun.*, 2015, **51**, 2518–2521.
22 M. U. Anu Prathap, S. Sun, C. Wei and Z. J. Xu, *Chem. Commun.*, 2015, **51**, 4376–4379.
23 J.-Y. Liao, B.-X. Lei, H.-Y. Chen, D.-B. Kuang and C.-Y. Su, *Energy Environ. Sci.*, 2012, **5**, 5750–5757.
24 J. Lee, S. H. Hwang, J. Yun and J. Jang, *ACS Appl. Mater. Interfaces*, 2014, **6**, 15420–15426.
25 S. Son, S. H. Hwang, C. Kim, J. Y. Yun and J. Jang, *ACS Appl. Mater. Interfaces*, 2013, **5**, 4815–4820.
26 I. G. Yu, Y. J. Kim, H. J. Kim, C. Lee and W. I. Lee, *J. Mater. Chem.*, 2011, **21**, 532–538.
27 Q. Zhang, D. Myers, J. Lan, S. A. Jenekhe and G. Cao, *Phys. Chem. Chem. Phys.*, 2012, **14**, 14982–14998.
28 S. Ito, P. Liska, P. Comte, R. Charvet, P. Pechy, U. Bach, L. Schmidt-Mende, S. M. Zakeeruddin, A. Kay, M. K. Nazeeruddin and M. Gratzel, *Chem. Commun.*, 2005, 4351–4353, DOI: 10.1039/B505718C.
29 S. H. Hwang, J. Yun and J. Jang, *Adv. Funct. Mater.*, 2014, **24**, 7619–7626.
30 J. Yun, S. H. Hwang and J. Jang, *ACS Appl. Mater. Interfaces*, 2015, **7**, 2055–2063.
31 J.-W. Choi, H. Kang, M. Lee, J. S. Kang, S. Kyeong, J.-K. Yang, J. Kim, D. H. Jeong, Y.-S. Lee and Y.-E. Sung, *RSC Adv.*, 2014, **4**, 19851–19855.

